ASM Sc. J., 21(1), 2026

https://doi.org/10.32802/asmscj.2026.0329

Investigation of Polypropylene Nanofiller Multi-Element Oxide Insulation Material for Mitigating Electrical Breakdown in High-Voltage Insulation Applications

A. Azmi[1*], N.A. Othman[2] and M.A.N.A. Md Nadzir [3]

[1]*Faculty of Electrical Engineering, Universiti Teknologi Malaysia, 81310, Skudai Johor, Malaysia*

[2]*Faculty of Electrical and Electronic Engineering, Universiti Tun Hussein Onn Malaysia. Batu Pahat, 86400 Johor, Malaysia*

[3]*APD Global Sdn Bhd, Level 23, Ilham Tower, No.8, Jalan Binjai, 50450 Kuala Lumpur, Malaysia.*

This paper examines the dielectric behaviour of pure polypropylene (PP) and its nanocomposites modified with 2 wt% of different multielement oxide nanofillers which is magnesium aluminate ($MgAl_2O_4$), calcium carbonate ($CaCO_3$), and zinc ferrite ($ZnFe_2O_4$). Differential scanning calorimetry (DSC) and Fourier-transform infrared spectroscopy (FTIR) were employed to assess thermal and chemical characteristics, respectively. The results indicate that pure PP demonstrates the highest direct current (DC) breakdown strength, reaching about 327 kV/mm. However, the breakdown strength drops to 271 kV/mm when 2 wt% $CaCO_3$ is added, with further reductions observed for $ZnFe_2O_4$ (239 kV/mm) and $MgAl_2O_4$ (174 kV/mm). These reductions are believed to be due to morphological changes introduced by the nanofillers, which act as nucleating agents, as confirmed by DSC analysis. Overall, the study emphasises that the type of nanofiller plays a decisive role in shaping the dielectric performance of PP-based composites.

Keywords: high voltage insulation; nanocomposites; multi-element oxide

I. INTRODUCTION

The growing demand for reliable high-voltage insulation materials has intensified research into advanced polymer nanocomposites. Among these, polypropylene (PP) has emerged as a leading candidate for high-voltage direct current (HVDC) cable insulation due to its high thermal stability, superior dielectric breakdown strength, low dielectric loss, recyclability, mechanical strength, and potential for space-charge suppression (Angalane and Kasinathan, 2022; Azmi *et al.*, 2021a; Azmi *et al.*, 2021b; Azmi *et al.*, 2022; Abbas *et al.*, 2020). However, unfilled PP faces limitations in dielectric breakdown strength and space charge accumulation under extreme electrical stresses (Azmi *et al.*, 2022; Adnan *et al.*, 2021). To address these challenges, the incorporation of multi-element oxide nanofillers has been widely explored to enhance the electrical and physical properties of PP-based insulation materials.

Recent studies have demonstrated that the addition of nanofillers such as magnesium aluminate ($MgAl_2O_4$), calcium carbonate ($CaCO_3$), and zinc ferrite ($ZnFe_2O_4$) can significantly influence the dielectric properties of PP nanocomposites (Alyabyev *et al.*, 2007). It had been reported in (Alyabyev *et al.*, 2007) that by adding $MgAl_2O_4$ as nanofillers tend to reduce the breakdown strength of PP due to permittivity mismatch and increased water absorption. Meanwhile, $CaCO_3$ and its surface-modified forms which is known as $CaCO_3T$ can significantly increase breakdown strength, with 1 wt% $CaCO_3T$ raising the value to 300±7 kV mm^{-1} compared to unfilled PP. This improvement is attributed to better dielectric compatibility, optimized interfacial interactions, and the formation of deep charge

*Corresponding author's e-mail: aizat.azmi@utm.my

traps at the polymer-filler interface, which suppress space charge accumulation and mitigate field distortion.

Although $ZnFe_2O_4$ nanofillers have been less studied in polypropylene (PP), they have demonstrated the ability to enhance dielectric properties in other polymer matrices. This enhancement is achieved by introducing additional charge trapping sites and modifying charge carrier dynamics, which is evidenced by shifts in Fourier-transform infrared spectroscopy (FTIR) absorption bands and increased dielectric constants (Alsulami, Alharbi & Keshk, 2022; Baca-Bocanegra *et al.*, 2022; Bezy *et al.*, 2024). Despite these promising advances, the structure-property relationships governing these enhancements remain insufficiently understood, particularly for multi-element oxide systems.

All aforementioned nanocomposites are believed to increase the insulation breakdown strength due to optimized interfacial interactions and reduced water absorption. These improvements result from deep charge traps formed at the polymer-filler interfaces, which help mitigate field distortion and reduce charge injection. The improvement in breakdown strength is closely linked to the nanofillers' dielectric constant, surface chemistry, and ability to form deep charge traps at the polymer-filler interface. $CaCO_3$ and its surface-modified forms tend to provide better dielectric compatibility and interfacial properties than $MgAl_2O_4$, while $ZnFe_2O_4$ offers promising semiconducting and magnetic characteristics that may further enhance electrical insulation performance.

$MgAl_2O_4$ is characterized by strong ionic bonding between magnesium and aluminum cations and oxygen anions, which contributes to its dielectric behavior. It has a relatively low dielectric loss and moderate dielectric constant approximately 6 to 8 in the MHz frequency range (Bhattu, Acevedo and Shnain, 2024). However, $MgAl_2O_4$ nanofillers tend to reduce the breakdown strength of PP nanocomposites. This reduction is attributed to local electric field intensification caused by the permittivity mismatch between $MgAl_2O_4$ and PP, as well as the presence of surface hydroxyl groups that can increase water absorption, leading to charge accumulation and early breakdown. Additionally, agglomeration of $MgAl_2O_4$ nanoparticles at higher loadings diminishes the beneficial interfacial effects (Carrero *et al.*, 2015).

$CaCO_3$ has a dielectric constant closer to that of PP, it effectively reduces local field distortion (Casci Ceccacci *et al.*, 2019). Thus, $CaCO_3$ nanofillers improve the breakdown strength of PP nanocomposites more effectively than $MgAl_2O_4$. Its surface properties and interaction with the polymer matrix help form deep charge traps at the interface, which suppress space charge accumulation and reduce charge injection. These traps enhance dielectric strength by mitigating electrical stress concentration. Surface modification of $CaCO_3$ like $CaCO_3$T further optimises interfacial bonding and reduces water absorption, leading to even higher breakdown strength (Abbas *et al.*, (2020).

$ZnFe_2O_4$ is a spinel ferrite structurally similar to $MgAl_2O_4$ which possesses semiconducting properties and moderate dielectric constants. It exhibits semiconducting behavior and moderate dielectric constants, with its electrical and magnetic properties strongly influenced by cation distribution and synthesis methods. $ZnFe_2O_4$ nanofillers can contribute to improved charge trapping due to their electronic structure and magnetic properties, which influence charge carrier dynamics at the interface. This can lead to enhanced breakdown strength by limiting charge mobility and reducing electrical treeing (Baca-Bocanegra *et al.*, 2022). However, detailed studies specific to $ZnFe_2O_4$ in PP nanocomposites are less common, and its effectiveness depends on particle dispersion and surface chemistry (Dhaka *et al.*, 2024).

To address this gap, this study systematically investigates the effects of $MgAl_2O_4$, $CaCO_3$, and $ZnFe_2O_4$ nanofillers on the chemical, thermal, and dielectric properties of PP nanocomposites. This paper extends our recent works (Azmi *et al.*, 2022; Abbas *et al.*, 2020; Alyabyev *et al.*, 2007) by systematically investigating the effects of different multi-element oxides at a fixed loading of 2 wt%, with particular emphasis on their influence on thermal, chemical, and dielectric breakdown strength. FTIR is employed to analyse chemical interactions, differential scanning calorimetry (DSC) is used to assess melting and cooling behaviour, and DC breakdown strength measurements are performed to evaluate electrical performance. The objectives are to quantify improvements in breakdown strength, understand filler dispersion and interfacial interactions, and elucidate the

mechanisms underlying dielectric enhancement for advanced HVDC insulation applications.

II. MATERIALS AND METHOD

Pure polypropylene (PP) and PP-based nanocomposites incorporating $MgAl_2O_4$, $CaCO_3$, and $ZnFe_2O_4$ were fabricated using a Brabender melt mixer shown in Figure 1. The mixing process was conducted at a rotor speed of 50 rpm, a temperature of 180 °C, and a mixing time of 10 minutes. To prepare thin-film specimens with a thickness of 100 µm, the compounded materials were subsequently melt-pressed using a hydraulic laboratory press under a load of 3 tons at 180 °C. The pressed films were then allowed to cool naturally under ambient laboratory conditions. For clarity and consistency, all prepared samples are designated using the general notation "P/F/A," where P denotes the polymer matrix, F indicates the type of nanofiller, and A represents the corresponding nanofiller loading (see Table 1).

Figure 1. Brabender melt mixer .

Table 1. Sample designation.

Sample (P/F/A)	Polymer (P)	Filler (F)	Amount (A)
PP/0/0	PP	N/A	N/A
PP/$CaCO_3$/2	PP	$CaCO_3$	2 wt%
PP/$ZnFe_2O_4$/2	PP	$ZnFe_2O_4$	2 wt%
PP/$MgAl_2O_4$/2	PP	$MgAl_2O_4$	2 wt%

Differential scanning calorimetry (DSC) is a highly suitable and widely accepted analytical technique for investigating the thermal properties of materials, such as melting and crystallisation behaviours. The method provides precise and quantitative data on phase transitions, which are critical for understanding the thermal stability, purity, and structural characteristics of the samples. In this study, employing the Perkin Elmer DSC6 instrument as shown in Figure 2 ensures reliable and reproducible results due to its sensitivity and accuracy. Each test involved sealing approximately 5 mg of sample in aluminium pans to minimise sample loss and ensure uniform heating. Conducting the measurements under a nitrogen atmosphere prevents oxidative degradation during heating, preserving the integrity of the samples.

Figure 2. Perkin Elmer DSC6.

The DSC protocol consisted of two stages: first, the sample was heated from 60 °C to 180 °C at a rate of 10 °C/min to assess its melting behaviour; this was followed by a cooling cycle from 180 °C back to 60 °C at the same rate to evaluate crystallisation behaviour. The chosen heating and cooling rates of 10 °C/min strike a balance between experimental efficiency and resolution of thermal events, allowing clear identification of melting and crystallisation peaks without excessive thermal lag (Dissado *et al.*, 1984; Du *et al.*, 2020). Data obtained from the scans were processed using Pyris software provided by Perkin Elmer. Instrument calibration was carried out using high-purity indium to secure accuracy in temperature and enthalpy measurements, as indium's well-characterised melting point and enthalpy serve as reliable standards. Therefore, in this work a certified melting point of 156.6 °C and a melting enthalpy of 28.45 J/g was used whereas the estimated measurement uncertainties were ±1 °C for temperature and ±3% for enthalpy values.

Fourier Transform Infrared (FTIR) spectroscopy is a widely accepted and powerful technique for chemical characterisation because it provides detailed information about molecular vibrations and functional groups present in materials. In this work, Shimadzu IRTracer-100 FTIR spectrometer equipped with a mid-infrared triglycine sulphate (MIRTGS) detector shown in Figure 3 was used.

This setup provides high sensitivity and stability, which enhances the detection of subtle spectral features.

Figure 3. Shimadzu IRTracer-100 Fourier Transform Infrared.

Analysing both nanopowder and thin-film samples allows comprehensive characterisation of the material in different physical forms, which can influence molecular interactions and structural properties. The 100 µm thickness for thin films was selected in this work to balance sufficient sample absorption while avoiding excessive attenuation or scattering of the infrared beam (Inoue *et al.*, 2018; Leong *et al.*, 2005). To obtain accurate FTIR spectra, data were collected over the spectral range of 500 to 4000 cm^{-1} (Shirota *et al.*, 2017), encompassing the mid-infrared region where the fundamental vibrational modes of most organic and inorganic compounds are found. This range allows for the effective identification of key functional groups. Apart from that, a resolution of 4 cm^{-1} was used as optimal for resolving overlapping peaks while maintaining a reasonable signal-to-noise ratio. Averaging 8 scans per sample improves the signal quality by reducing random noise, thereby increasing the reliability and reproducibility of the spectral data.

DC breakdown measurements were performed using a dielectric strength testing apparatus in accordance with the ASTM D3755 standard. Each test specimen had a nominal thickness of 100 µm. During testing, the sample was placed between two steel ball electrodes, each with a diameter of 6.3 mm, and submerged in mineral oil to prevent surface discharges. All measurements were conducted at ambient room temperature. The breakdown voltages obtained were recorded and analysed statistically using the two-parameter Weibull distribution to assess the dielectric strength of the samples.

The DC breakdown test was conducted to evaluate the breakdown characteristics of unfilled polypropylene PP and PP-based nanocomposites incorporating $MgAl_2O_4$, $CaCO_3$, and $ZnFe_2O_4$. A BAUR PGK 110B AC/DC high voltage test set, capable of delivering up to 110 kV DC, was employed for this purpose. The test setup for DC breakdown was structurally similar to that used for AC breakdown testing, with the primary difference being the inclusion of a rectifier to convert AC to DC voltage. A schematic representation of the DC breakdown testing configuration, highlighting the major components involved, is provided in Figure 4.

A stepwise DC voltage was applied to the samples, increasing by 2 kV every 20 seconds, until electrical breakdown occurred. For each type of sample, a total of 15 breakdown events were recorded to ensure statistical reliability. The collected breakdown voltage data were subsequently analysed using the two-parameter Weibull distribution method.

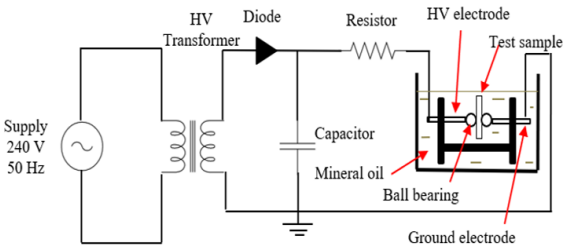

Figure 4. Illustration of the experimental setup employed for measuring the direct-current (DC) breakdown strength of the samples.

Weibull analysis was employed in this study to evaluate the breakdown strength of polypropylene (PP)-based nanocomposites containing $MgAl_2O_4$, $CaCO_3$, and $ZnFe_2O_4$. The statistical treatment of the breakdown data adhered to the guidelines outlined in IEC 62539, which provides a standard framework for analysing electrical insulation failure data. The Weibull probability distribution offers a robust graphical method for interpreting failure behaviour, delivering reliable insights into dielectric breakdown characteristics. This distribution is characterised by two key parameters: the scale parameter (α), which reflects the characteristic breakdown strength, and the shape parameter (β), which indicates the data's dispersion. The cumulative distribution function of the Weibull model, presented in Equations (1) illustrates the probabilistic behaviour of breakdown strength. The graphical representation of failure

data using this method enables accurate and meaningful analysis of insulation performance.

In the Weibull distribution, P(E) represents the probability of dielectric breakdown occurring at a given electric field strength x (kV/mm). The scale parameter α corresponds to the electric field strength at which there is a 63.2% probability of failure, and it shares the same unit as xx. The shape parameter β characterises the distribution's form, with higher values of β indicating reduced variability in the breakdown strength data. For analysis, the breakdown values are arranged in ascending order, and a corresponding probability P(E) is assigned to each data point. A straight line is then fitted to the data using the maximum likelihood estimation (MLE) method, which provides more accurate and statistically reliable estimates of the parameters α and β. The cumulative probability of failure, P(E)P(E)P(E), can be estimated using the median rank method, as presented in Equation (2).

$$P(E) = 1 - exp\left\{-\left(\frac{x}{\alpha}\right)^{\beta}\right\} \quad (1)$$

$$P(E) = \frac{i - 0.3}{m + 0.4} \quad (2)$$

In this method, i denotes the rank order of the failure event, while m represents the total number of tests conducted. The median rank approach is widely recognised for its reliable approximation of cumulative failure probability and its consistency across various data analysis techniques. Figure 5 demonstrates the research flow chart.

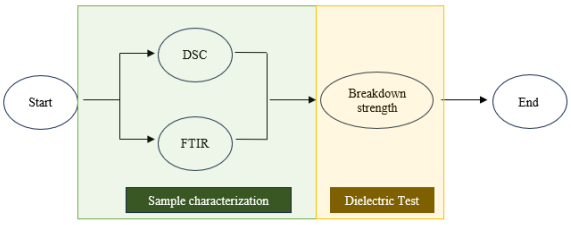

Figure 5. Research flowchart.

III. RESULT AND DISCUSSION

Figure 6 presents the FTIR spectra of pure PP (black colour) and PP nanocomposites containing 2 wt% of $MgAl_2O_4$ (red colour), $CaCO_3$ (yellow colour), and $ZnFe_2O_4$ (purple colour) nanofiller. In the reference spectrum for pure PP, characteristic absorption bands are observed between 2836 cm^{-1} and 2950 cm^{-1}, corresponding to the stretching vibrations of methyl ($-CH_3$) and methylene ($-CH_2-$) groups. Additionally, bending vibrations of these groups are evident in the range of 844 cm^{-1} to 1458 cm^{-1}. With the incorporation of $MgAl_2O_4$ nanoparticles into the PP matrix, a distinct absorption peak appears at 686 cm^{-1}, attributed to $MgAl_2O_4$. This peak becomes increasingly prominent with higher $MgAl_2O_4$ content, indicating its effective integration (Tabaza, 2014). Similarly, the introduction of $CaCO_3$ leads to the emergence of new absorption bands at 873 cm^{-1} and 707 cm^{-1}, which are characteristic of the carbonate filler (Zaman *et al.*, 2013).

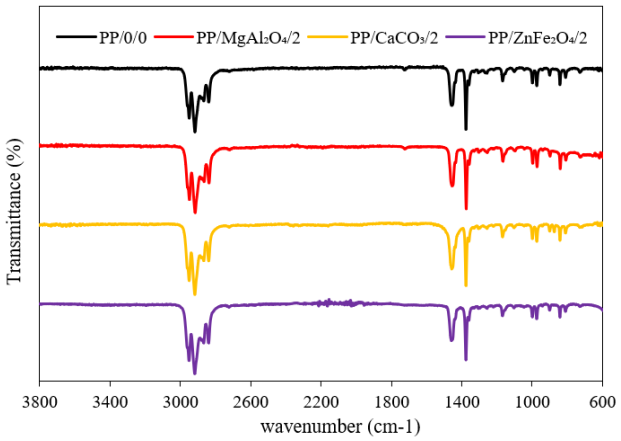

Figure 6. FTIR spectra comparing unfilled PP and PP nanocomposites.

In the case of $ZnFe_2O_4$-filled composites, the FTIR spectra retain the fundamental absorption bands of PP, suggesting that the polymer's chemical structure remains intact. Furthermore, additional bands are detected in the 400–600 cm^{-1} region, corresponding to Zn–O and Fe–O stretching vibrations, thereby confirming the successful incorporation and dispersion of $ZnFe_2O_4$ nanoparticles within the polymer matrix (Zhang *et al.*, 2008).

Figure 7 illustrates the differential scanning calorimetry (DSC) melting and cooling behaviour of pure PP and its nanocomposites containing 2 wt% of $MgAl_2O_4$, $CaCO_3$, and $ZnFe_2O_4$, with the corresponding data summarised in Table 2. The peak melting temperatures (Tm) which denoted in dotted pattern have demonstrated nearly identical for all samples that averaging around 162 °C. This indicates the characteristic of the α-crystalline form of PP. This similarity

in melting profiles suggests that the incorporation of the nanofillers does not significantly alter the lamellar thickness within the polymer matrix. In contrast, the DSC cooling curves (denoted with diagonal brick) reveal distinct differences: while pure PP exhibits a crystallisation temperature (Tc) of approximately 118 °C, the addition of $MgAl_2O_4$, $CaCO_3$, and $ZnFe_2O_4$ results in an increase in Tc. This enhancement indicates that the nanofillers function as nucleating agents, promoting earlier crystallisation and thereby influencing the overall crystalline morphology of the composites (Zhang *et al.*, 2022).

A Weibull statistical analysis was performed to assess the DC breakdown strength of pure PP and its nanocomposites incorporating 2 wt% of $MgAl_2O_4$, $CaCO_3$, and $ZnFe_2O_4$, as summarised in Table 3 and illustrated in Figure 8.

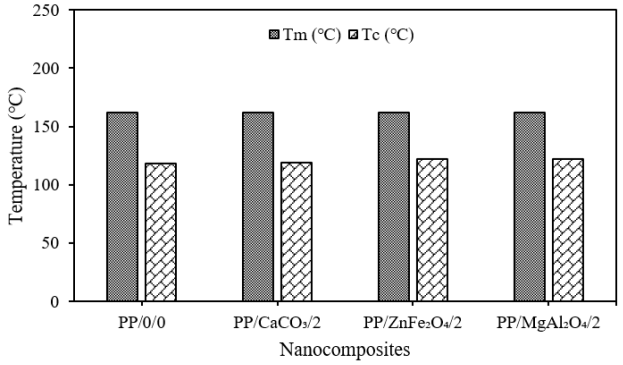

Figure 7. Comparison of the melting and cooling of PP and PP nanocomposites.

Table 2. DSC melting and cooling parameters.

Sample	Tm (℃)	Tc (℃)
PP/0/0	162	118
PP/CaCO3/2	162	119
PP/ZnFe2O4/2	162	122
PP/MgAl2O4/2	162	122

Weibull distribution parameters characteristic breakdown strength (α) and shape parameter (β) effectively quantify the breakdown strength and reliability of PP and its nanocomposites (Zhou *et al.*, 2020). Pure PP demonstrated the highest α of 323 ± 10 kV/mm, accompanied by a β of 15 ± 6, reflecting high reliability and uniformity in its breakdown behaviour. The introduction of 2 wt% $ZnFe_2O_4$ yielded a marginal reduction in breakdown strength, with the PP/$ZnFe_2O_4$/2 nanocomposite recording a value of 239 kV/mm, indicating minimal impact (26% reduction compared to pure PP). However, the addition of $CaCO_3$ resulted in a notable decrease in breakdown strength to 271 kV/mm (16% reduction compared to pure PP). A further decline was observed with $MgAl_2O_4$, registering breakdown strengths of 176 kV/mm (46% reduction compared to pure PP). These variations are attributed to morphological alterations induced by the nanofillers, which act as nucleating agents, as corroborated by DSC results.

The improvements in dielectric breakdown strength observed, especially for $CaCO_3$-filled composites, suggest promising applications in critical HV insulation components i.e., cable sheaths. Enhanced breakdown performance can potentially extend the operational lifetime of such equipment, reduce maintenance requirements, and contribute to more compact insulation designs.

Table 3. DC Breakdown parameters.

Sample	α (kV/mm)	β
PP/0/0	323 ± 18	17 ± 8
PP/CaCO3/2	271 ± 19	7 ± 2
PP/ZnFe2O4/2	239 ± 22	5 ± 2
PP/MgAl2O4/2	176 ± 6	13 ± 5

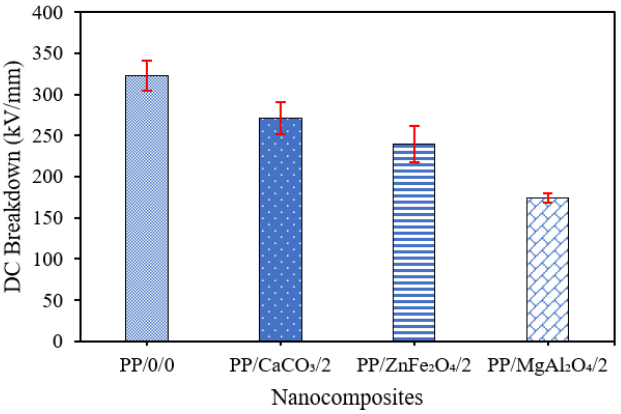

Figure 8. Comparison of the DC breakdown strength of PP and PP nanocomposites.

By aligning material properties with the stringent demands of practical high-voltage systems, these nanocomposites hold potential as sustainable and efficient solutions for advanced insulation applications.

IV. CONCLUSION

The breakdown strength analysis of polypropylene (PP) nanocomposites demonstrates that the incorporation of $MgAl_2O_4$, $CaCO_3$, and $ZnFe_2O_4$ nanoparticles significantly affects their dielectric performance. Among the tested systems, the addition of $CaCO_3$ had the least impact, with a breakdown strength of 271 kV/mm, while PP/$ZnFe_2O_4$/2 and PP/$MgAl_2O_4$/2 exhibited lower values of 239 kV/mm and 176 kV/mm, respectively. The notable reduction in DC breakdown strength, particularly in the $MgAl_2O_4$-filled composite, is attributed to morphological changes, as evidenced by differential scanning calorimetry (DSC) analysis. Furthermore, Fourier-transform infrared spectroscopy (FTIR) confirmed successful integration of the nanofillers within the PP matrix, indicating effective nanocomposite formation. Overall, this study highlights the critical role of nanofiller selection in tailoring the dielectric properties of PP nanocomposites for high-voltage insulation applications. While $CaCO_3$ nanofillers demonstrate promise in maintaining or improving breakdown strength, $MgAl_2O_4$ may require surface modification or optimised loading to mitigate adverse effects on morphology and electrical performance. $ZnFe_2O_4$ exhibits intermediate behaviour, suggesting potential for further exploration given its semiconducting and magnetic properties that could be harnessed to improve charge trapping and dielectric stability. Future research should focus on evaluating the long-term reliability and durability of these PP nanocomposites under realistic operational conditions. Aging studies, including thermal and electrical aging, thermal cycling, and moisture exposure tests, are essential to understand potential degradation mechanisms affecting dielectric performance. Incorporating computational modelling and simulation approaches could provide deeper insights into breakdown phenomena and allow optimisation of filler types, concentrations, and surface modifications to further enhance material performance. Specifically, surface treatment of $MgAl_2O_4$ nanoparticles may mitigate adverse effects on morphology and electrical properties observed in this study.

V. ACKNOWLEDGEMENT

This research was funded by the Matching Grant (Vote No. Q841) sponsored by Universiti Tun Hussein Onn Malaysia (UTHM). The authors gratefully acknowledge the financial assistance and access to facilities provided by UTHM, which were instrumental in the successful completion of this project. Appreciation is also extended to Universiti Teknologi Malaysia (UTM) for granting access to its facilities through UTMER, Q.J130000.3823.42J23.

VI. REFERENCES

Angalane, SK & Kasinathan, E 2022, 'Influence of nanofiller concentration on polypropylene nanocomposites for high voltage cables', Journal of Electrical Engineering, vol. 73, pp. 174–181.

Azmi, A, Lau, K, Ahmad, N, Abdul-Malek, Z, Tan, C & Ching, K 2021, 'Structure and breakdown properties of polypropylene-based nanocomposites', in 2021 IEEE International Conference on the Properties and Applications of Dielectric Materials (ICPADM), IEEE, pp. 202–205.

Azmi, A, Lau, KY, Ahmad, NA, Abdul-Malek, Z, Tan, CW, Ching, KY et al. 2021, 'Structure-dielectric property relationship in polypropylene/multi-element oxide nanocomposites', IEEE Transactions on Nanotechnology, vol. 20, pp. 377–385.

Azmi, A, Lau, K, Ahmad, N, Abdul-Malek, Z, Tan, C, Ching, KY et al. 2022, 'Dielectric properties of thermally aged polypropylene nanocomposites', IEEE Transactions on Dielectrics and Electrical Insulation, vol. 29, pp. 543–550.

Abbas, Q, Murtaza, G, Muhammad, N, Ishfaq, M, Iqbal, H, Asad, A et al. 2020, 'Structural, dielectric and magnetic properties of ($ZnFe_2O_4$/Polystyrene) nanocomposites synthesized by micro-emulsion technique', Ceramics International, vol. 46, pp. 5920–5928.

Adnan, M, Abdul-Malek, Z, Lau, KY & Tahir, M 2021, 'Polypropylene-based nanocomposites for HVDC cable insulation', IET Nanodielectrics, vol. 4, pp. 84–97.

Alyabyev, AJ, Loseva, NL, Gordon, LK, Andreyeva, IN, Rachimova, GG, Tribunskih, VI et al. 2007, 'The effect of changes in salinity on the energy yielding processes of

Chlorella vulgaris and Dunaliella maritima cells', Thermochimica Acta, vol. 458, pp. 65–70.

Alsulami, QA, Alharbi, LM & Keshk, SM 2022, 'Synthesis of a graphene oxide/$ZnFe_2O_4$/polyaniline nanocomposite and its structural and electrochemical characterization for supercapacitor application', International Journal of Energy Research, vol. 46, pp. 2438–2445.

Baca-Bocanegra, B, Martínez-Lapuente, L, Nogales-Bueno, J, Hernández-Hierro, JM & Ferrer-Gallego, R 2022, 'Feasibility study on the use of ATR-FTIR spectroscopy as a tool for the estimation of wine polysaccharides', Carbohydrate Polymers, vol. 287, article 119365.

Bezy, NA, Jasvy, S, Jeba, SV, Sebastiammal, S & Fathima, AL 2024, 'Dielectric properties $ZnFe_2O_4$ nanofiller on the commercial epoxy composites', Jordan Journal of Physics, vol. 17, pp. 245–252.

Bhattu, M, Acevedo, R & Shnain, A 2024, 'A comprehensive review on the synthesis routes, properties and potential applications of $ZnFe_2O_4$ ferrites', in E3S Web of Conferences, vol. 491, article 02014.

Carrero, J, Oliva, V, Navascués, B, Borrull, F & Galià, M 2015, 'Determination of antioxidants in polyolefins by pressurized liquid extraction prior to high performance liquid chromatography', Polymer Testing, vol. 46, pp. 21–25.

Casci Ceccacci, A, Cagliani, A, Marizza, P, Schmid, S & Boisen, A 2019, 'Thin film analysis by nanomechanical infrared spectroscopy', ACS Omega, vol. 4, pp. 7628–7635.

Dhaka, S, Panda, M, Singh, V, Prajapat, P, Choudhary, B & Kumar, S 2024, 'Tailoring the structural and dielectric properties of $ZnFe_2O_4$ through annealing temperature', Physica B: Condensed Matter, vol. 674, article 415574.

Dissado, LA, Fothergill, JC, Wolfe, SV & Hill, RM 1984, 'Weibull statistics in dielectric breakdown: Theoretical basis, applications and implications', IEEE Transactions on Electrical Insulation, vol. EI-19, no. 3, pp. 227–233.

Du, C, Guo, H-H, Zhou, D, Chen, H-T, Zhang, J, Liu, W-F et al. 2020, 'Dielectric resonator antennas based on high quality factor $MgAl_2O_4$ transparent dielectric ceramics', Journal of Materials Chemistry C, vol. 8, pp. 14880–14885.

Inoue, H, Yoneda, S, Kato, M, Ohsugi, I & Kobayashi, T 2018, 'Examination of oxidation resistance of Mg_2Si thermoelectric modules at practical operating temperature', Journal of Alloys and Compounds, vol. 735, pp. 828–832.

Leong, Y, Bakar, MA, Mohd. Ishak, Z & Ariffin, A 2005, 'Effects of filler treatments on the mechanical, flow, thermal, and morphological properties of talc and calcium carbonate filled polypropylene hybrid composites', Journal of Applied Polymer Science, vol. 98, pp. 413–426.

Shirota, M, van Limbeek, MA, Lohse, D & Sun, C 2017, 'Measuring thin films using quantitative frustrated total internal reflection (FTIR)', The European Physical Journal E, vol. 40, pp. 1–9.

Tabaza, WAI 2014, Synthesis and Characterization of $MgAl_2O_4$ and $(Mg_xZn_{1-x})Al_2O_4$ Mixed Spinel Phosphors, master's thesis, University of the Free State.

Zaman, HU, Hun, PD, Khan, RA & Yoon, K-B 2013, 'Effect of surface-modified nanoparticles on the mechanical properties and crystallization behavior of PP/$CaCO_3$ nanocomposites', Journal of Thermoplastic Composite Materials, vol. 26, pp. 1057–1070.

Zhang, J, Wu, DX, Chang, XH, Lu, TC, Jiang, YH & Zhu, JG 2008, 'Dielectric properties of $MgAl_2O_4$ transparent nano-ceramic', Key Engineering Materials, vol. 368, pp. 412–413.

Zhang, Y, Shi, K, Zang, C, Wei, W, Xu, C & Zha, J 2022, 'Improved insulation properties of polypropylenes in HVDC cables using aqueous suspension grafting', Materials, vol. 15, article 6298.

Zhou, Y, Hu, S, Yuan, C, Hu, J, Li, Q & He, J 2020, 'Recyclable polypropylene-based insulation materials for HVDC cables: Progress and perspective', CSEE Journal of Power and Energy Systems.